ELSEVIER

Journal of Chromatography A, 876 (2000) 63–73

JOURNAL OF CHROMATOGRAPHY A

www.elsevier.com/locate/chroma

Optimization of ion-exchange displacement separations II. Comparison of displacement separations on various ion-exchange resins

Venkatesh Natarajan, Steven M. Cramer*

Department of Chemical Engineering, Rensselaer Polytechnic Institute, Troy, NY 12180, USA

Received 26 July 1999; received in revised form 7 January 2000; accepted 26 January 2000

Abstract

A variety of stationary-phase materials are currently available for the chromatographic purification of biomolecules. However, the effect of various resin characteristics on the performance of displacement chromatography has not been studied in depth. In Part I, a novel iterative scheme was presented for the rapid optimization of displacement separations in ion-exchange systems. In this article, the optimization scheme is employed to identify the optimum operating conditions for displacement separations on various ion-exchange resin materials. In addition, the effect of different classes of separation problems (e.g., diverging, converging or parallel affinity lines) on the performance of displacement separations is also presented. The solid film linear driving force model is employed in concert with the Steric Mass Action isotherm to describe the chromatographic behavior in these systems. The results presented in this article provide insight into the effects of resin capacity and efficiency as well as the type of separation problem on the performance of various ion-exchange displacement systems. © 2000 Elsevier Science B.V. All rights reserved.

Keywords: Optimization; Displacement chromatography; Steric mass action; Ion-exchange chromatography

1. Introduction

Over the course of the past decade, the displacement mode of chromatography has received significant attention as a high-resolution and a high-throughput preparative tool [1–5]. The efficacy of displacement chromatography for the purification of proteins from industrial process streams has recently been demonstrated [6,7]. Conventionally, large polyelectrolytes have been employed as displacers in ion-exchange systems [8–11]. However, it has recently been demonstrated that low-molecular-weight displacers can also be effectively employed in these systems [12]. A variety of low-molecular-weight displacers have been identified, including amino acids [12] and antibiotics [13]. In addition, low-molecular-weight displacers have been successfully employed for high-resolution separations [14].

There has been a dramatic increase in the number and variety of stationary-phase materials over the past decade. However, there is currently a lack of understanding of the effect of various resin characteristics (e.g., stationary-phase chemistry, capacity, transport properties) on displacement separations.

*Corresponding author. Tel.: +1-518-276-6198; fax: +1-518-276-4030.

E-mail address: crames@rpi.edu (S.M. Cramer)

0021-9673/00/$ – see front matter © 2000 Elsevier Science B.V. All rights reserved.
PII: S0021-9673(00)00139-4

Stationary-phase characteristics are expected to impact two aspects of displacement chromatography: (a) the affinity of displacer molecules; and (b) the yields and production rates achievable with displacement separations. Recently, Shukla et al. [15] have studied the affinities of homologous series of low-molecular-weight displacers on a variety of ion-exchange resins. This body of work has provided significant insight into the effect of stationary-phase chemistry on displacer affinity and has provided a tool for the rational design of low-molecular-weight displacer molecules for various stationary-phase chemistries. In order to study the effect of a particular stationary-phase material on the performance of displacement separations, however, one needs to carry out mathematical modeling and optimization of these separations. Recently, it has been demonstrated that the solid film linear driving force model [16] in conjunction with the Steric Mass Action (SMA) [17] isotherm can accurately describe the chromatographic behavior in protein ion-exchange displacement systems over a wide range of operating conditions [18]. In Part I, an algorithm was presented for the optimization of displacement separations [19]. In this article, the algorithm will be employed to optimize displacement separations on three different stationary-phase materials for different classes of separation problems. The work presented in this paper provides insight into the efficacy of various resin materials for displacement chromatography.

2. Theory

2.1. Classification of separation problems in displacement systems

The SMA formalism [17] is a three-parameter model for the description of multicomponent protein–salt equilibrium in ion-exchange systems. This isotherm was presented in Part I [19]. Unlike the Langmuir isotherm, the SMA model is a non-constant separation factor formalism. The separation factor in the SMA model is a function of the salt concentration and is given by [18]:

$$\alpha_{ij} \equiv \frac{Q_i/C_i}{Q_j/C_j} = \frac{K_i}{K_j}\left(\frac{\bar{Q}_1}{C_1}\right)^{\nu_i-\nu_j} \quad (1)$$

Since the SMA formalism is a non-constant separation factor system, it becomes difficult to a priori categorize the degree of difficulty of a given separation. Eq. (1) reduces to the following equation under dilute (i.e. linear) conditions:

$$\alpha_{ij,\text{linear}} = \frac{K_i}{K_j}\left(\frac{\Lambda}{C_1}\right)^{\nu_i-\nu_j} \quad (2)$$

Eq. (2) is a measure of the closeness of the linear retention plots of solutes *i* and *j*. However, the use of this linear separation factor to quantify the degree of difficulty of separation in a non-linear system such as displacement is inappropriate since the selectivity under non-linear conditions may be quite different.

The dynamic affinity, λ, of a solute is defined as [20]:

$$\lambda_i = \left(\frac{K_i}{\Delta}\right)^{1/\nu_i} \quad (3)$$

where

$$\Delta = \frac{Q_{\text{displacer}}}{C_{\text{displacer}}} \quad (4)$$

For displacement systems, it is appropriate to employ the ratio of the dynamic affinities of the solutes to characterize the degree of difficulty of the separation [18]:

$$\alpha_{i,j}^{\text{disp}} = \frac{\lambda_i}{\lambda_j} = \frac{(K_i)^{1/\nu_i}}{(K_j)^{1/\nu_j}}(\Delta)^{(\nu_i-\nu_j)/(\nu_i\nu_j)} \quad (5)$$

Eq. (5) defines a separation factor for displacement systems. For a given Δ, $\alpha_{i,j}^{\text{disp}}$ is constant and is a measure of the closeness of the dynamic affinities (λ) of the two solutes. The affinity ranking plot is a graphical representation of Eq. (5) and plots the logarithm of the dynamic affinity (λ) versus the logarithm of Δ (Fig. 1). As can be seen in the figure, the relative proximity of the affinity lines of the solutes can be employed as a measure of the degree of difficulty of their separation. Thus, a mixture of solutes 1 and 2 is expected to pose a challenging separation problem. On the other hand, a mixture of solutes 1 and 3 is expected to be an easy separation problem. Furthermore, different classes of separation problems can be identified based on the relative slopes of the affinity lines. These are illustrated in Fig. 2a–c. As can be seen in these figures, one could

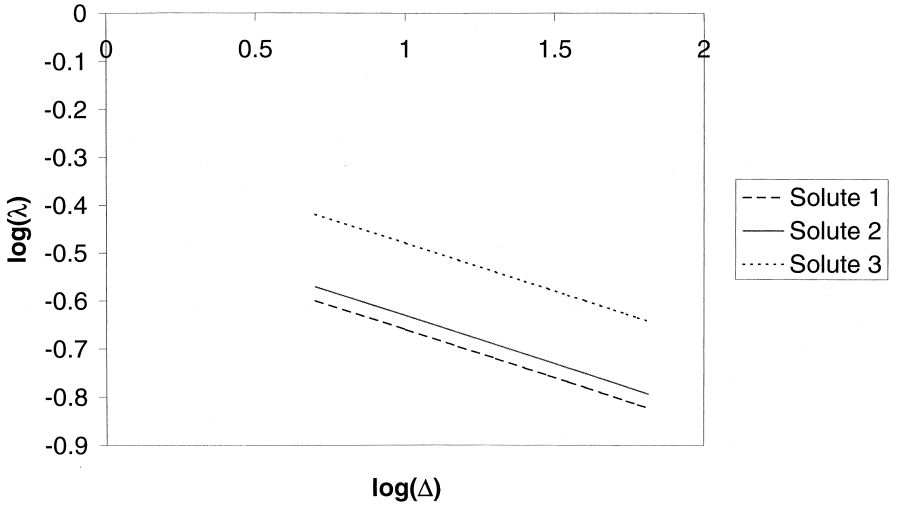

Fig. 1. Affinity ranking plots for three hypothetical solutes.

classify displacement separations as converging (Fig. 2a; the vertical distance between the affinity lines decreases with increasing Δ), parallel (Fig. 2b; the vertical distance between the affinity lines is invariant with Δ) or diverging (Fig. 2c; the vertical distance between the affinity lines increases with increasing Δ) problems.

2.2. Mass transport equations

It turns out that, for the stationary-phase materials employed in this study, the Peclet number was >500, rendering the axial dispersion effects insignificant. Thus, in this article, the solid film linear driving force model described in Part I was employed without the Peclet number.

2.3. Numerical solution of model equations

Finite difference techniques were employed to solve Eqs. (6) and (7). As the SMA isotherm is implicit, a Newton–Raphson technique was used in each step for the equilibrium calculations. The temporal terms were discretized using forward differences, while the convection and diffusion terms were discretized using backward and central differences, respectively.

The discretized equations were solved subject to the following stability criteria [18]:

$$\frac{\Delta\tau}{\mathrm{Pe}_i(\Delta x)^2} < 0.2 \tag{8}$$

$$\frac{\Delta\tau}{\Delta x} < 1 \tag{9}$$

A FORTRAN code was written to solve the above equations. The program was run on an IBM RS/6000 workstation using IBM FORTRAN under the AIX 4.0 operating system.

2.4. Chromatographic optimization

The objective function, decision variables, constraints and parameters employed in the optimization of displacement systems were described in detail in Part I [19]. The iterative scheme outlined in Part I [19] was employed to optimize the displacement separations. Binary feed mixtures are examined in this article. The production rate (PR) of the higher-affinity solute (solute 2) was the objective function:

$$\mathrm{PR}_2 = \frac{C_{2,\mathrm{f}} V_{\mathrm{f}} Y_2}{t_{\mathrm{cyc}} V_{\mathrm{sp}}} \tag{10}$$

where the yield, Y_2, is defined as:

$$Y_i = \frac{\int_{t_1}^{t_2} C_i \, \mathrm{d}t}{C_{i,\mathrm{f}} t_{\mathrm{f}}} \tag{11}$$

The cycle time in the objective function includes

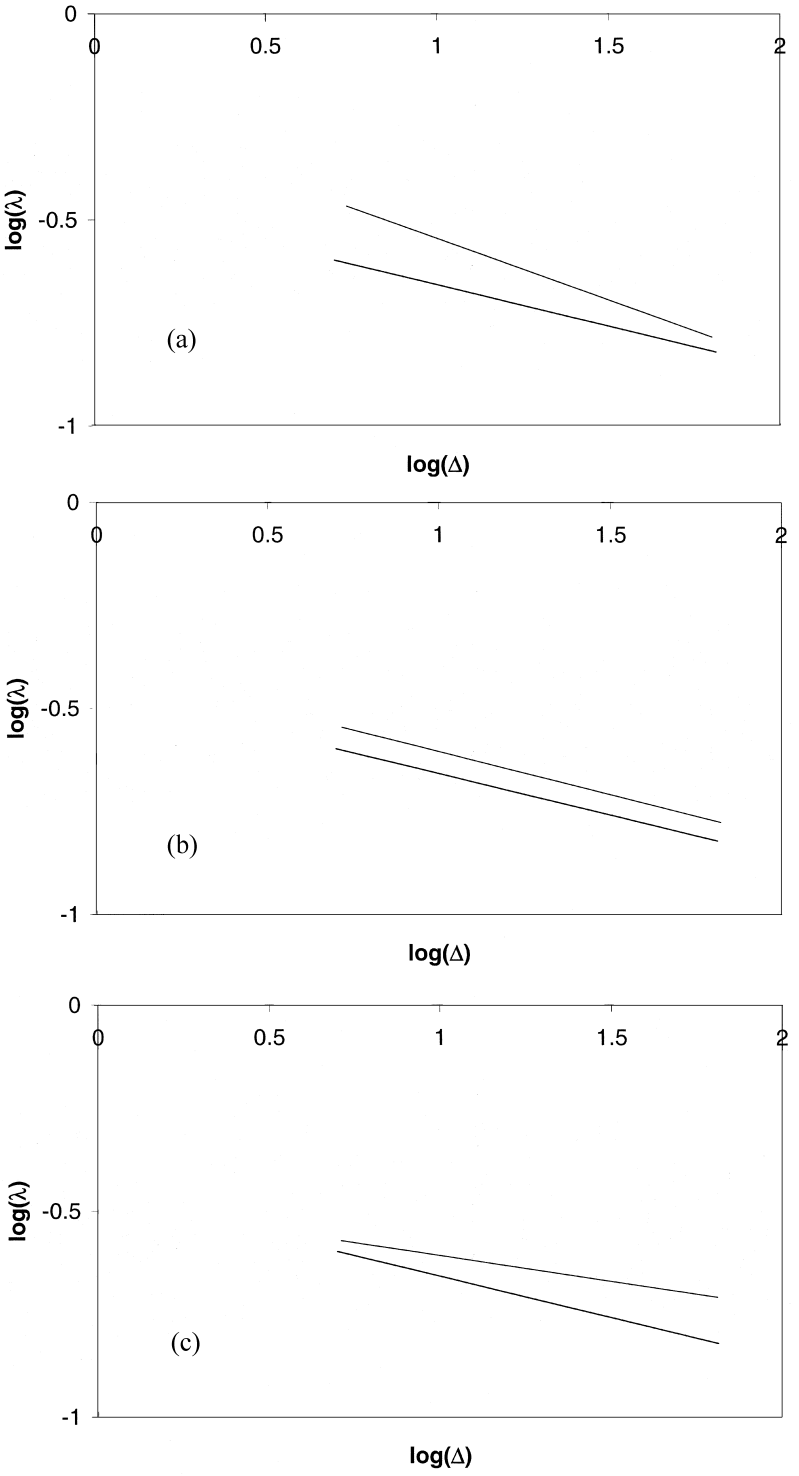

Fig. 2. Classification of separation problems based on the relative slopes of the affinity lines. (a) Converging affinity lines, (b) parallel affinity lines, and (c) diverging affinity lines.

Table 1
Details of the optimization study

	Bounds		
	HP Sepharose	8 μm Waters	40 μm Waters
Decision variables			
Initial salt concentration	20–250 mM[a]	20–200 mM[a]	20–200 mM[a]
Flow-rate	0.1–2 mL/min	0.1–2 mL/min	0.1–4 mL/min
Δ	5–50	5–50	5–50
Constraints			
Purity	>95%	>95%	>95%
Yield	>80%	>80%	>80%
Maximum protein concentration	<4 mM	<4 mM	<4 mM

[a] Based on the highest salt concentration at which elution does not occur [22].

the time required for regeneration. It was assumed that seven column volumes of regenerant were required for complete regeneration. Thus, the cycle time employed throughout this article is defined as:

$$\tau_{cyc} = \tau_f + \tau_{sep} + 7 \quad (12)$$

The decision variables were the feed load, the initial salt concentration, the flow-rate and Δ. Appropriate constraints of yield, purity and solubility were imposed on these systems. The parameters for a given stationary-phase material were the pH, SMA and transport parameters and the feed composition. The optimization details and the SMA parameters of the separation problems employed in this article are listed in Tables 1 and 2, respectively.

3. Results and discussion

The properties of the stationary-phase materials examined in this article are listed in Table 3. The values of the lumped mass transport parameters and the steric factors are representative of those obtained with proteins on these resin materials [18]. As can be seen from the table, the Q_{max} on the HP Sepharose material is significantly higher than that on the polymethacrylate materials. In addition, the lumped mass transport parameter on the 34 μm HP Sepharose material is significantly higher than that on the 40 μm Waters material.

On each of these resin materials, three hypothetical separation problems were considered. As described earlier, these separation problems differed in the variation of their separation factor as a function of the operational parameter, Δ. The parameters for the three separation problems along with the SMA parameters for the displacer chosen for these separations are listed in Table 2. The parameters of the displacer are those of a typical low-molecular-weight, high-affinity solute. Fig. 3 illustrates the variation of the separation factor (described above) of the three separations as a function of Δ. The performance of displacement chromatography with these classes of separation problems on all the resins listed in Table 3 will now be examined.

Displacement separations at a given level of loading are affected by the flow-rate, initial salt

Table 2
Parameters for the separation problems employed in this study[a]

Separation problem	Solute 1	Solute 2	Average separation factor
Parallel	$\nu = 5$, $K = 0.006$	$\nu = 5$, $K = 0.0084$	1.06
Converging	$\nu = 5.08$, $K = 0.0038$	$\nu = 5$, $K = 0.006$	1.07
Diverging	$\nu = 5$, $K = 0.006$	$\nu = 5.2$, $K = 0.006$	1.07

[a] For all three cases, displacer: $\nu = 4$, $K = 10$, steric factor 3.56. For all three cases, feed composition 0.51 mM of each solute.

Table 3
Characteristics of the resins employed in this study

Resin	Chemistry, pore size	Total porosity	Bed capacity (m*M*)	Steric factor of solutes	Q_{max} (m*M*)	k_m (min^{-1}) (solute, displacer)
8 μm Waters	PMMA, 1000 Å	0.75	600	40	13.3	360, 720
40 μm Waters	PMMA, 1000 Å	0.75	600	40	13.3	36, 72
34 μm HP Sepharose	Sepharose, exclusion limit: 4×10^6 MW (globular protein)	0.85	1200	15	60	102, 204

concentration and Δ. As described in Part I [19], the optimization of displacement separations at a given level of loading can be achieved by performing two optimizations in series: (a) optimization of the initial salt concentration and (b) the simultaneous optimization of the flow-rate and Δ. Fig. 4a–c illustrate the variation of the optimum values of the initial salt concentration, flow-rate and Δ as a function of the level of loading. These plots were generated for the separation problem with parallel affinity lines on the HP Sepharose resin. However, the trends suggested by these plots are independent of both the type of separation problem and the resin material. As can be seen in Fig. 4a, the optimum initial salt concentration decreases with the level of loading and finally becomes independent of the feed load. Operation at high initial salt concentration results in lower protein concentrations and broader zones in the final displacement train. Thus, at low feed loadings, the optimum initial salt concentration is relatively high. In fact, at the lowest level of loading, the optimum initial salt concentration was close to the upper bound in all the cases examined in this article. However, high salt concentrations limit the amount of material that can be loaded onto the column. Thus, the optimum initial salt concentration decreases with increasing feed load. Finally, beyond a certain level of loading, one is constrained to operate at the lowest possible salt concentration.

Fig. 4b and c illustrate the variation of the optimum flow-rate and optimum Δ as a function of the level of loading. As can be seen in these figures, the optimum flow-rate is relatively constant up to a certain level of loading and decreases rapidly after

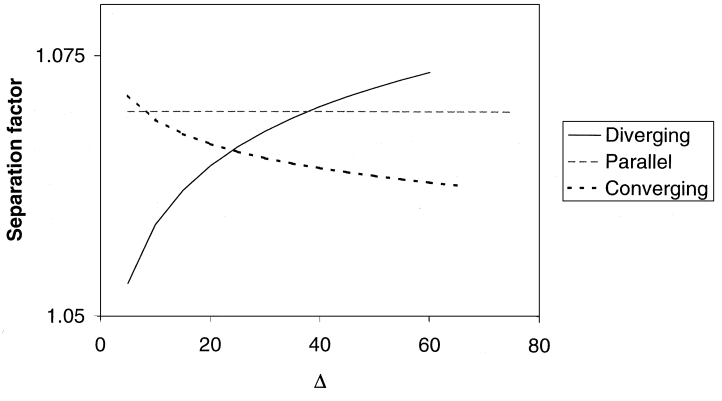

Fig. 3. Variation of the separation factor of the separation problems considered in this article as a function of Δ. The separation factor was computed using Eq. (5) and the parameters listed in Table 2.

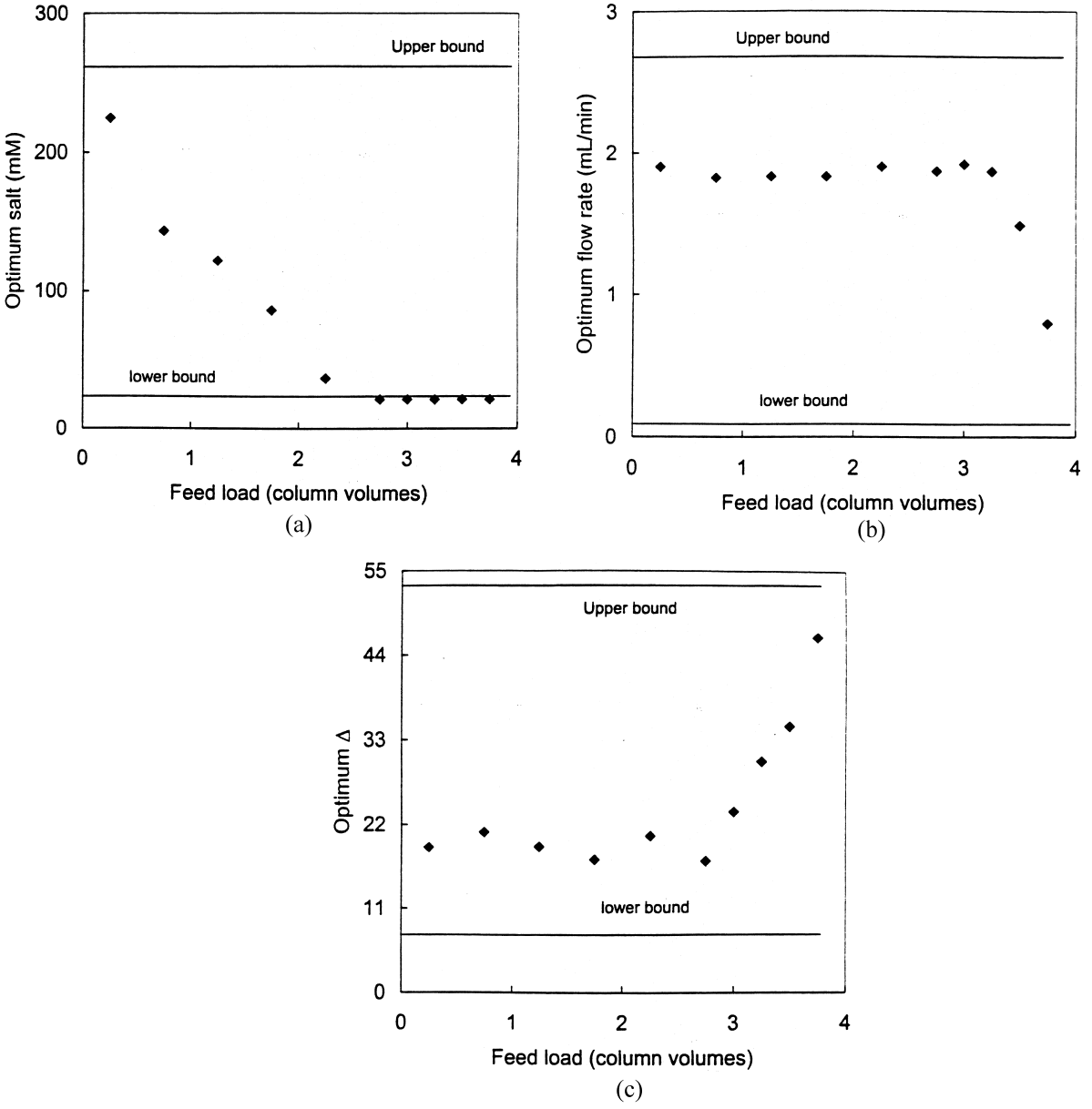

Fig. 4. Dependence of the optimum values of the decision variables on the level of loading. These results are specifically for the separation problem with parallel affinity lines on the HP Sepharose material. However, the trends suggested by these plots are independent of the resin material and the class of separation problem. (a) Optimum salt concentration, (b) optimum flow-rate, and (c) optimum Δ.

that point. The variation of the optimum Δ as a function of loading is almost a mirror image of the optimum flow-rate trend. Increasing the flow-rate results in an increase in the shock layer thickness which lowers the yields obtainable in these systems. To counter this, one has to increase the Δ used for the separation (i.e. lower the displacer concentration) to broaden the zones in the final displacement train and to improve the yield. However, beyond a certain flow-rate, the increase in the shock layer thickness

cannot be compensated by further increases in Δ. The value of this limiting flow-rate is dependent on both the type of separation problem and the resin material employed for the separation. Thus, at low and moderate levels of loading, the production rate is maximized by operating close to this flow-rate. Consequently, the optimum flow-rate (and, thus, the optimum Δ) is relatively independent of the level of loading. However, at high levels of loading, non-development occurs, resulting in lowered yields. Thus, one needs to both reduce the flow-rate and increase the Δ at these high levels of loading to enable the yield constraint to be satisfied.

The displacement performance of the three resins for the three classes of separation problems is summarized in Table 4a–c. As seen in the table, for a given separation problem, the optimum Stanton number is more or less the same on all three resins. This implies that the optimum Stanton number is primarily dependent on the separation problem at hand and not on the resin material being employed. The Stanton number ($k_m L/u$) is a dimensionless group that relates the diffusional transport rate to the convective rate. It essentially establishes the magnitude of the linear velocities that can be employed for a given separation problem on a given resin. The average optimum Stanton number on the three resins is listed in Table 4d. As can be seen in the table, the optimum Stanton numbers for the converging and diverging problems are significantly different. The reason for this is as follows: for separation problems with converging affinity lines, the optimum Δ's lie at the lower end. Thus, the final protein concentrations are higher, and, as a result, the solute zones are narrower. Consequently, for the converging problem, one is restricted to operate at lower flow-rates which enables the minimization of the shock layer thickness. On the other hand, for diverging problems, the optimum Δ's are relatively high, resulting in lower protein concentrations and broader zones. Thus, diverging problems can accommodate higher flow-rates. Thus, the optimum Stanton numbers for a converging problem are significantly higher than those for a diverging one. As expected, the optimum Stanton numbers for the parallel class of separation problem lie in between.

The optimum Δ's, on the other hand, are dependent not only on the type of separation problems but also on the resin material. On the two Waters resins, the optimum Δ's are comparable, while on the HP Sepharose material, the optimum Δ's are significantly higher. The reason for this behavior lies in the

Table 4
Summary of optimization results

Separation problem	Optimum Δ	Optimum linear velocity (cm/min)	Optimum Stanton number	Optimum loading factor (%)	Optimum salt (mM)	Optimum PR
(a) 8 μm Waters						
Parallel	16.2	7.7	351	25.2	20.9	9.53e−2
Converging	13.7	6.5	393	26.4	20.9	8.31e−2
Diverging	39.7	8.9	303	23	20.9	7.42e−2
(b) 40 μm Waters						
Parallel	15	0.75	362	25.2	20.9	9.5e−3
Converging	10	0.7	386	20.7	20.9	8.4e−3
Diverging	35.9	0.88	307	25.2	20.9	7.37e−3
(c) 34 μm HP Sepharose						
Parallel	25.6	2.44	355	28.9	20.9	1.32e−1
Converging	22.8	2.25	385	26.5	20.9	1.14e−1
Diverging	46	3.02	287	31.3	20.9	1.4e−1
(d) Average optimum Stanton numbers for the three types of problems						
Parallel			356			
Converging			388			
Diverging			299			

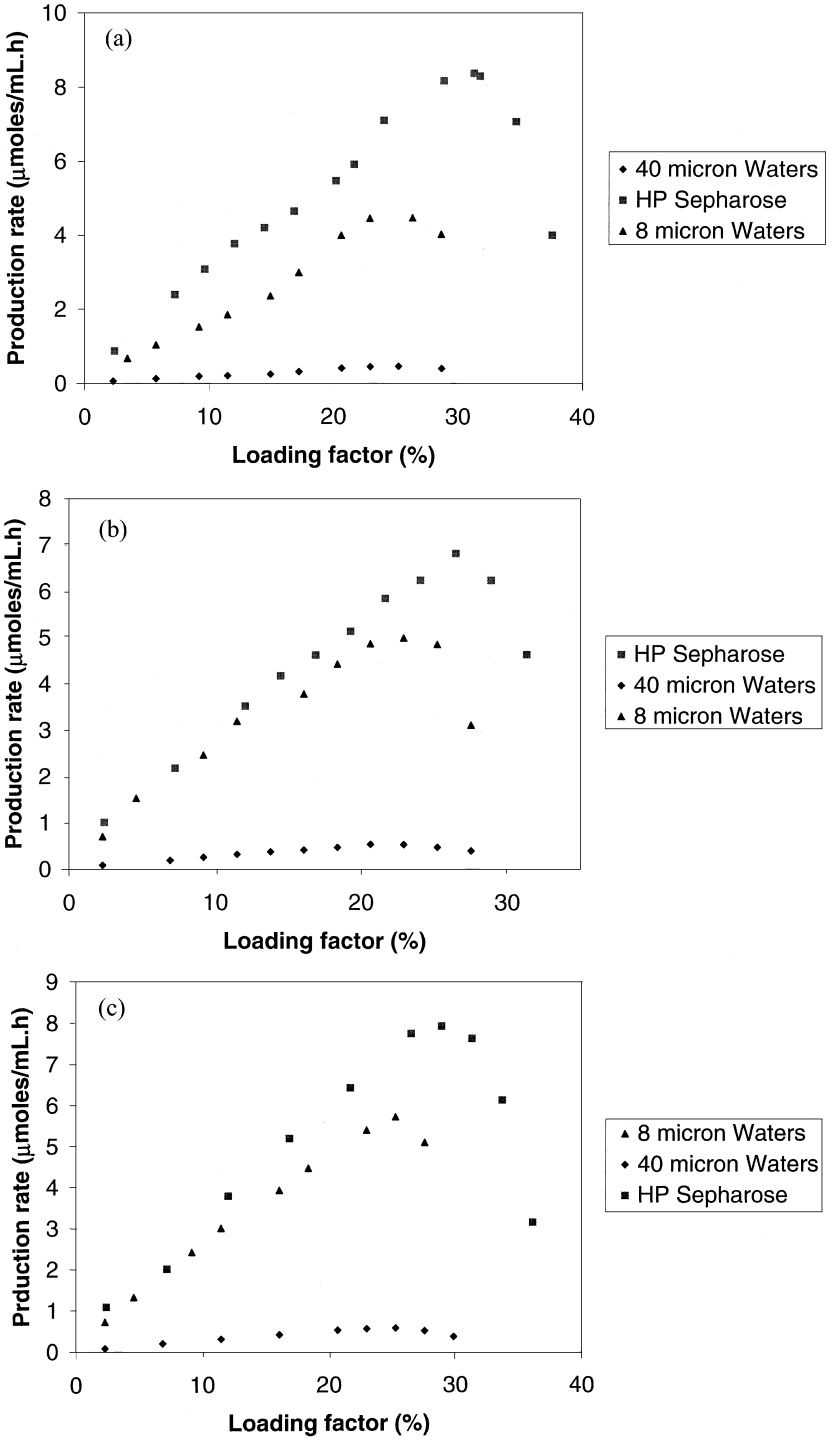

Fig. 5. Variation of the optimum production rate as a function of the loading factor for the three separation problems. (a) Separation problem with diverging affinity lines, (b) separation problem with converging affinity lines, and (c) separation problem with parallel affinity lines.

differences in Q_{max} between the two types of resins. The final protein concentrations will be higher on the HP Sepharose resin since its Q_{max} is highest. Thus, at a fixed Stanton number, higher Δ's need to be employed on the HP Sepharose material to satisfy the yield constraint. As can be seen in Table 4a–c, the optimum Δ is highest for the problem with diverging affinity lines on all three resins. This is expected since the separation factor increases with increasing Δ for this case (Fig. 3). On the other hand, for the converging parallel problem, the optimum Δ's are lower. The optimum Δ's for the parallel problem lie closer to those for the converging problem since the difficulty of separation remains independent of the magnitude of Δ. Thus, although the average separation factors for all three separation problems are almost identical (Table 2), the class of separation problem (i.e., diverging, converging, parallel) plays an important role in the identification of optimum conditions.

Fig. 5a–c illustrate the variation of the production rate as a function of the loading factor, which is a measure of the percent total capacity of the resin that is loaded (note: each point on these plots represents the optimum production rate at a given level of loading). The loading factor, L_f, is defined as:

$$L_f = \frac{100\tau_f V_0 \sum_{i=2}^{NC-1} C_f}{(1-\varepsilon_t)SLQ_{max}} \quad (13)$$

The symbols are defined in the Nomenclature section. As seen in Fig. 5, the optimum loading factor is higher on the HP Sepharose resin than on either of the Waters resins. In addition, the production rate obtainable on the HP Sepharose resin is higher than those obtainable on both of the Waters resins for all three types of problems. This is a surprising result since it suggests that a large-particle system (34 μm HP Sepharose) can perform better than a small-particle system (8 μm Waters) for displacement separations. As seen in Table 3, the lumped mass transport coefficient on the HP Sepharose resin is about three times greater than that of the 40 μm Waters resin. This enables operation at higher flow-rates. Thus, the optimum production rates on the HP Sepharose resin are higher than those on the 40 μm Waters. In addition, the Q_{max} of the HP Sepharose resin is more than four times greater than that on the Waters resins (Table 3). This allows higher loadings on the HP Sepharose material. Thus, a relatively large-particle-size material (34 μm HP Sepharose) is able to show better performance than a small-particle-size material (8 μm Waters). The poorest performance was obtained with the 40 μm Waters material. This indicates that, for resins with low capacities, it would be efficacious to operate with low particle sizes.

4. Conclusions

In this article, a novel iterative optimization routine has been employed to carry out the optimization of displacement systems. The optimization routine was applied to three different classes of separations on three different resin materials. The results suggest that the optimum Stanton number is dictated by the separation problem at hand and is relatively independent of the resin type. On the other hand, the characteristics of a resin play a very important role in the production rates achievable with a given separation problem. The results suggest that a resin with a high capacity may be particularly efficacious for displacement separations. The higher capacity can allow higher levels of loading and may also help improve mass transport characteristics by allowing for surface diffusion [21]. It has been demonstrated that a relatively large-particle-size material (34 μm HP Sepharose) can perform better than a small-particle-size material (8 μm Waters). The results presented in this article shed significant light upon the effect of resin characteristics on the performance of displacement separations.

5. Nomenclature

C	Mobile phase concentration (mM)
C_F	Feed concentration (mM)
D	Axial dispersion coefficient (cm^2 min^{-1})
K	Equilibrium constant
k_m	Lumped mass transfer coefficient
L	Length of column (cm)
L_f	Loading factor (%)
NC	Number of components in the system
Pe	Peclet number ($=Lu/D$) (dimensionless)

PR	Production rate (mmol/(mL min))
Q	Stationary phase concentration (=mmol adsorbed/mL solid phase) (mM)
Q^*	Stationary phase concentration at equilibrium with C (mM)
$\bar{Q}_1$	Concentration of bound salt that is not sterically shielded (mM)
$\hat{Q}_1$	Concentration of bound salt that is sterically shielded (mM)
Q_{max}	Maximum capacity of resin (mM)
S	Column cross-section area (cm^2)
St	Stanton number ($=k_m L/u$) (dimensionless)
t	Time (min)
t_0	Time taken for an inert tracer to traverse the column (min)
t_f	Loading time
u	Chromatographic velocity (cm min^{-1}) ($=u_0/\varepsilon$)
u_0	Superficial velocity (cm min^{-1})
V_0	Column void volume (mL)
Y	Yield
x	Axial distance along column (dimensionless)

5.1. Greek

α	Separation factor
β	Phase ratio ($=(1-\varepsilon)/\varepsilon$)
ε_t	Total porosity
λ	Dynamic affinity
ν	Characteristic charge
σ	Steric factor
τ	Dimensionless time ($=t/t_0$)
τ_f	Dimensionless feed time
τ_{sep}	Dimensionless separation time
Δ	Partition ratio
Λ	Bed capacity (mM)

5.2. Subscripts

i	Component number. $i=1$ refers to the salt counterion and $i=NC$ refers to the displacer

Acknowledgements

This research was funded by grant No. CTS-9416921 from the National Science Foundation.

References

[1] A.W. Liao, Z. El Rassi, D.M. LeMaster, Cs. Horvath, Chromatographia 24 (1987) 881.
[2] J. Frenz, Cs. Horvath, in: Cs. Horvath (Ed.), High Performance Liquid Chromatography — Advances and Perspectives, Academic Press, New York, 1988, p. 212.
[3] G. Subramanian, M.W. Phillips, S.M. Cramer, J. Chromatogr. 439 (1988) 341.
[4] S.C.D. Jen, N.G. Pinto, J. Chromatogr. Sci. 29 (1990) 478.
[5] G. Guiochon, S.G. Shirazi, A.M. Katti (Eds.), Fundamentals of Preparative and Nonlinear Chromatography, Academic Press, New York, 1994, p. 299.
[6] A.A. Shukla, R.L. Hopfer, E. Bortell, D. Chakrabarti, S.M. Cramer, Biotechnol. Prog. 14 (1998) 92.
[7] K.A. Barnthouse, W. Trompeter, R. Jones, P. Inampudi, R. Rupp, S.M. Cramer, J. Biotechnol. 66 (2-3) (1998) 125.
[8] J.A. Gerstner, S.M. Cramer, Biotechnol. Prog. 8 (1992) 540.
[9] G. Jayaraman, S.D. Gadam, S.M. Cramer, J. Chromatogr. 630 (1993) 53.
[10] J.A. Gerstner, S.M. Cramer, BioPharm 5 (1992) 42.
[11] E.A. Peterson, A.R. Torres, Anal. Biochem. 130 (1983) 271.
[12] A. Kundu, S. Vunnum, G. Jayaraman, S.M. Cramer, Biotechnol. Bioeng. 48 (1995) 452.
[13] A. Kundu, S. Vunnum, S.M. Cramer, J. Chromatogr. A 707 (1995) 57.
[14] A. Kundu, S.M. Cramer, Anal. Biochem. 248 (1997) 1.
[15] A.A. Shukla, S.S. Bae, J.A. Moore, S.M. Cramer, J. Chromatogr. A 827 (1998) 295.
[16] H.-K. Rhee, N.R. Amundson, Chem. Eng. Sci. 29 (1974) 2049.
[17] C.A. Brooks, S.M. Cramer, AIChE J. 38 (1992) 1969.
[18] V. Natarajan, S.M. Cramer, AIChE J. 45 (1999) 27.
[19] V. Natarajan, B.W. Bequette, S.M. Cramer, J. Chromatogr. A 876 (2000) 41.
[20] C.A. Brooks, S.M. Cramer, Chem. Eng. Sci. 51 (1996) 3847.
[21] V. Natarajan, S.M. Cramer, Sep. Sci. Tech. (2000) in press.
[22] S.R. Gallant, S.M. Cramer, J. Chromatogr. A 771 (1997) 9.